5176 *Biochemistry* **2010,** *49,* 5176–5187
DOI: 10.1021/bi100399e

BIOCHEMISTRY
including biophysical chemistry & molecular biology
Article

Increasing the Conformational Entropy of the Ω-Loop Lid Domain in Phosphoenolpyruvate Carboxykinase Impairs Catalysis and Decreases Catalytic Fidelity[†,‡]

Troy A. Johnson and Todd Holyoak*

Department of Biochemistry and Molecular Biology, The University of Kansas Medical Center, Kansas City, Kansas 66160

Received March 15, 2010; Revised Manuscript Received April 26, 2010

ABSTRACT: Many studies have shown that the dynamic motions of individual protein segments can play an important role in enzyme function. Recent structural studies of the gluconeogenic enzyme phosphoenolpyruvate carboxykinase (PEPCK) demonstrate that PEPCK contains a 10-residue Ω-loop domain that acts as an active site lid. On the basis of these structural studies, we have previously proposed a model for the mechanism of PEPCK catalysis in which the conformation of this mobile lid domain is energetically coupled to ligand binding, resulting in the closed conformation of the lid, necessary for correct substrate positioning, becoming more energetically favorable as ligands associate with the enzyme. Here we test this model by introducing a point mutation (A467G) into the center of the Ω-loop lid that is designed to increase the entropic penalty for lid closure. Structural and kinetic characterization of this mutant enzyme demonstrates that the mutation has decreased the favorability of the enzyme adapting the closed lid conformation. As a consequence of this shift in the equilibrium defining the conformation of the active site lid, the enzyme's ability to stabilize the reaction intermediate is weakened, resulting in catalytic defect. This stabilization is initially surprising, as the lid domain makes no direct contacts with the enolate intermediate formed during the reaction. Furthermore, during the conversion of OAA to PEP, the destabilization of the lid-closed conformation results in the reaction becoming decoupled as the enolate intermediate is protonated rather than phosphorylated, resulting in the formation of pyruvate. Taken together, the structural and kinetic characterization of A467G-PEPCK supports our model of the role of the active site lid in catalytic function and demonstrates that the shift in the lowest-energy conformation between open and closed lid states is a function of the free energy available to the enzyme through ligand binding and the entropic penalty for ordering of the 10-residue Ω-loop lid domain.

Phosphoenolpyruvate carboxykinase (PEPCK)[1] catalyzes the reversible decarboxylation and phosphorylation of OAA to form PEP as shown in Scheme 1. While in vitro the reaction is freely reversible, the overall consensus is that in most organisms PEPCK operates primarily in the direction of PEP synthesis. PEPCK is a metal-requiring enzyme demonstrating an absolute requirement for divalent cations for activity. Mn^{2+} is the most activating cation in the GTP-dependent isoforms (*1*−*4*). In addition, a second divalent metal ion is required for the reaction, as the metal−nucleotide complex is the true substrate. In higher eukaryotes, PEPCK is present as both a cytosolic (cPEPCK) and mitochondrial (mPEPCK) isoform, with the relative distribution of these two isoforms being species-dependent. In its biological role, cPEPCK functions as a key cataplerotic enzyme; in addition to its well-characterized role in gluconeogenesis, PEPCK participates in glyceroneogenesis and triglyceride biosynthesis as well as the synthesis of serine (reviewed in ref *5*). In contrast, the role of mPEPCK in metabolic function is less understood.

In general, the structural data on PEPCK illustrate the presence of a specialized cationic active site, dominated by the juxtaposition of the two aforementioned divalent metal ions and the positioning of specific lysine and arginine residues, that is well suited to carry out both the decarboxylyation/carboxylation and phosphoryl transfer half-reactions as well as the stabilization of the enolate intermediate postulated to form along the stepwise reaction pathway (*6*). Because of the inherent reactivity of the enolate intermediate, primarily its energetically favorable protonation resulting in pyruvate, we have suggested that the protection or stabilization of the enolate by the enzyme is key to the reversible nature of the PEPCK-catalyzed reaction (Scheme 1) (*6*).

[†]T.H. acknowledges support from National Center for Research Resources (Grant P20 RR17708). Portions of this research were conducted at the Stanford Synchrotron Radiation Laboratory (SSRL), a national user facility operated by Stanford University on behalf of the U.S. Department of Energy, Office of Basic Energy Sciences. The SSRL Structural Molecular Biology Program is supported by the Department of Energy, Office of Biological and Environmental Research, and by the National Institutes of Health, National Center for Research Resources, Biomedical Technology Program, and the National Institute of General Medical Sciences.

[‡]Coordinates and structure factors have been deposited in the RCSB Protein Data Bank as entries 3MOE, 3MOF, and 3MOH.

*To whom correspondence should be addressed. Phone: (913) 588-0795. Fax: (913) 588-7440. E-mail: tholyoak@kumc.edu.

[1]Abbreviations: ASU, asymmetric unit; βSP, 3-sulfopyruvate; cPEPCK, cytosolic phosphoenolpyruvate carboxykinase; DTT, dithiothreitol; GDP, guanosine 5′-diphosphate; GTP, guanosine 5′-triphosphate; GTPγS, guanosine 5′-*O*-(γ-thio)triphosphate; IDP, inosine 5′-diphosphate; ITP, inosine 5′-triphosphate; ITPγS, inosine 5′-*O*-(γ-thio)triphosphate; NCS, noncrystallographic symmetry; OAA, oxaloacetic acid; PEG, polyethylene glycol; PEP, phosphoenolpyruvate; PEPCK, phosphoenolpyruvate carboxykinase; PGA, 2-phosphoglycolate; rmsd, root-mean-square deviation; TIM, triosephosphate isomerase; TLS, translation/libration/screw.

 Published on Web 05/17/2010

An informative aspect of the recent structural studies of the GTP-dependent isozyme from rat is the illumination of the previously unappreciated role of conformational changes occurring at the active site during the catalytic cycle (*6*−*9*). The most prevalent mobile feature illustrated by the structural work is a 10-residue Ω-loop lid domain, reminiscent of a similar domain in TIM (*10*−*13*). An essential role for this domain in PEPCK-mediated catalysis is suggested by the structural data for PEPCK demonstrating that only upon closure of the lid domain are the substrates positioned correctly for phosphoryl transfer to occur (*9*). In addition to the essential role lid closure is proposed to play in positioning the substrates for catalysis, closure of the lid may additionally sequester the enolate intermediate, allowing PEPCK-mediated catalysis to occur via the mechanism illustrated in Scheme 1.

The dynamic nature of lid opening and closing begs the question of what the energetic driving force for lid closure is and what specific role lid closure plays in the catalytic cycle. As the structural data demonstrate that no new direct contacts are made between the lid when it closes in the presence of substrates versus in their absence, we have previously proposed a model consistent with the notion originally proposed by Fersht (*14*). In this model, the thermodynamic favorability of the enzyme adapting the closed lid (active) state increases as ligands add to the enzyme, with a portion of their Gibbs free energy of binding being partitioned to the protein. This energy partitioning has the effect of remodeling the free energy profile for the protein and offsetting the entropic penalty associated with the lid assuming an ordered closed conformation rather than a conformationally dynamic open (inactive) state (*9*). Previous solid-state and solution NMR studies on TIM (*15*, *16*) are consistent with the model we propose for PEPCK lid motion (above and ref *9*), as these studies on TIM suggest that the position of the open−closed equilibrium is dependent on the nature of the bound ligand.

To further probe the role of lid closure in PEPCK catalytic function and to test our model, in which the penalty for the reduction in configurational entropy of the enzyme upon lid ordering is paid by the interaction free energy of substrates and/or intermediates, we have generated a lid mutation [A467G (Figure 1)] that is designed to increase the entropic penalty for ordering of the lid in the closed conformation. Structural and kinetic characterization of this mutant demonstrates that, consistent with our model for lid closure, the A467G mutation results in a decrease in the propensity for the lid to adapt its closed conformation. As a functional consequence, this disruption in the energetics of lid closure results in an observed decrease in the fidelity of the conversion of OAA to PEP through the decoupling of the reaction to pyruvate. In addition, even though the closed lid makes no direct contacts with the substrates, the kinetic data are consistent with the destabilization of the closed lid conformation resulting in PEPCK becoming less able to stabilize the enolate intermediate. This loss of enolate stabilization significantly impacts the kinetics of the reaction, resulting in a k_{cat}/K_M for OAA that is only 2% of the wild-type (WT) value.

MATERIALS AND METHODS

Materials. The nucleotides (GTP, GDP, IDP, ITP, and ADP) and 2-phosphoglycolate were purchased from Sigma. PEP and NADH were from Chem-Impex. DTT was from Gold Bio-Tech. HEPES buffer was from Research Organics. Oxalic acid was from Fluka. βSP was synthesized and purified as previously described (*17*). Glutathione Uniflow Resin was purchased from Clontech. HiQ, P6DG, and Chelex resins were from Bio-Rad. All other materials were of the highest grade commercially available.

Enzymes. Malate dehydrogenase (22976 units/mL, 50% glycerol solution) and lactate dehydrogenase (6000 units/mL, $AmSO_4$ suspension) were from Calzyme Laboratories. Pyruvate kinase (10 mg/mL, $AmSO_4$ suspension) was from Roche.

PEPCK Expression and Purification. Recombinant, WT rat cPEPCK was expressed and purified as previously described (*8*) with the following alterations. All buffers in the purification included 10 mM DTT and were treated with Chelex resin for 10 min prior to filter degassing. The molar extinction coefficient used to determine protein concentrations is 1.65 mL mg^{-1} as determined experimentally (*18*).

Generation of A467G PEPCK. Recombinant rat cPEPCK in PGEX-4T-2 was used as the starting vector to create the A467G mutation. The forward primer (5′-GAGGCCACCGC-TGGTGCAGAGCATAAGG-3′) and its reverse complement were utilized with the Stratagene Quik Change protocol. The resultant mutated DNA was isolated with a Hurricane cleanup kit from Gerard Biotech and subsequently sequenced to confirm the presence of the desired mutation and the absence of any additional mutations introduced via the polymerase chain reaction (PCR) protocol. The plasmid DNA was transformed into *Escherichia coli* BL-21(DE3) electro-competent cells for expression. Expression and purification of the A467G mutant followed the same protocol as the WT enzyme with the same modifications described above.

Crystallization. Crystals of the complexes of A467G PEPCK were obtained as previously described for the WT enzyme (*9*).

Data Collection. Data for the cryo-cooled A467G PEPCK−Mn^{2+}−βSP−Mn^{2+}GTP, and A467G PEPCK−Mn^{2+}−oxalate−Mn^{2+}GTP complexes maintained at 100 K were collected on beamline 11-1 of the Stanford Synchrotron Radiation Laboratory (Menlo Park, CA). Data for the A467G PEPCK−Mn^{2+}−PGA−Mn^{2+}GDP crystal maintained at 100 K were collected using a RU-H3R rotating copper anode X-ray generator with Blue

462 **G** 476
S E A T A A A E H K G K V I M

FIGURE 1: Sequence of the active site lid domain (residues 462−476). The site of introduction of the glycine (position 467) is indicated above the sequence.

Scheme 1: PEPCK-Catalyzed Interconversion of OAA and PEP

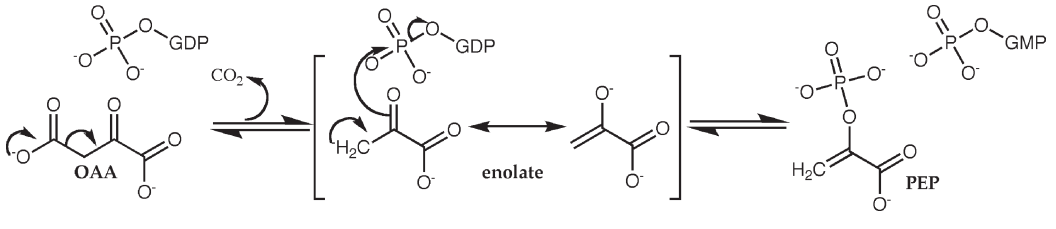

Table 1: Crystallographic Data and Model Statistics for the Structures of A467G PEPCK

	A467G PEPCK−Mn^{2+}−βSP−Mn^{2+}GTP	A467G PEPCK−Mn^{2+}−PGA−Mn^{2+}GDP	A467G PEPCK−Mn^{2+}−oxalate−Mn^{2+}GTP
wavelength (Å)	0.9	1.54	0.9
space group	$P2_1$	$P2_1$	$P2_1$
unit cell	a = 44.3 Å b = 119.1 Å c = 60.1 Å α = γ = 90.0° β = 111.2°	a = 62.1 Å b = 119.5 Å c = 87.0 Å α = γ = 90.0° β = 107.2°	a = 62.0 Å b = 119.6 Å c = 87.1 Å α = γ = 90.0° β = 106.9°
resolution limit (Å)	20.6−1.25	35.93−2.10	33.24−1.75
no. of unique reflections	152044	68697	118295
completeness[a] (%) (all data)	95.0 (67.2)	97.2 (80.3)	96.7 (94.9)
redundancy[a]	6.9 (3.5)	7.0 (4.9)	7.1 (6.9)
$I/\sigma_{(I)}$[a]	28.2 (2.1)	10.0 (1.6)	18.0 (2.3)
R_{merge}[a]	0.04 (0.46)	0.1 (0.59)	0.06 (0.55)
no. of ASU molecules	1	2	2
R_{free}[a]	17.4 (34.2)	24.7 (34.1)	22.8 (33.1)
R_{work}[a]	14.8 (32.7)	19.0 (28.2)	17.9 (29.3)
estimated coordinate error based on maximum likelihood (Å)	0.03	0.16	0.10
bond length rmsd (Å)	0.03	0.01	0.02
bond angle rmsd (deg)	2.6	1.5	1.5
Ramachandran statistics (preferred, allowed, outliers) (%)	96.9, 2.4, 0.7	96.4, 3.0, 0.6	96.5, 2.7, 0.8
state of active site lid	molecule A, open	molecule A, open molecule B, open	molecule A, 70% closed molecule B, open

[a]Values in parentheses represent statistics for data in the highest-resolution shells.

Confocal Osmic mirrors and a Rigaku Raxis IV^{++} detector. All data were integrated and scaled with HKL-2000 (*19*). Final data statistics are presented in Table 1.

Structure Determination and Refinement. The A467G enzyme structures were determined by the molecular replacement method using MOLREP (*20*) in the CCP4 package (*21*) and the previously determined rat cPEPCK structures of the same complexes [Protein Data Bank (PDB) entries 3DT4, 3DT7, and 3DTB] (*9*). For each complex, the molecular replacement solution was refined using Refmac5 followed by manual model adjustment and rebuilding using COOT (*22*). Ligand, metal, and water addition and validation were also performed in COOT. A final round of TLS refinement was performed for all models in Refmac5. A total of five groups per chain for the A467G PEPCK−Mn^{2+}−βSP−Mn^{2+}GTP and A467G PEPCK−Mn^{2+}−oxalate−Mn^{2+}GTP models were used as refinements using more than five groups per chain did not significantly improve R/R_{free}. A total of 20 groups per chain for the A467G PEPCK−Mn^{2+}−PGA−Mn^{2+}GDP model were used. The optimum TLS groups were determined by submission of the PDB files to the TLSMD server (http://skuld.bmsc.washington.edu/~tlsmd/) (*23*−*25*). Final model statistics are listed in Table 1.

Kinetic Experiments. All kinetic data were collected on a Cary 100 spectrophotometer equipped with a multicell changer and a temperature bath. PEPCK activity was assayed in both the physiological direction of PEP formation and the reverse direction of OAA formation using modifications of previously published assays (*1*, *18*, *26*). All assays were performed at 25 °C, in a final volume of 1 mL, and monitored spectrophotometrically by following the decrease in absorbance at 340 nm due to the oxidation of NADH. The oxidation of NADH was recorded in real time, to allow the calculation of a rate of enzyme activity from the extinction coefficient for NADH (*27*). In all kinetic assays, the concentrations of PEPCK utilized were 14−36 and 43−86 nM for the WT and A467G enzyme forms, respectively.

Assay A ($OAA + GTP \rightarrow PEP + CO_2 + GDP$). The decarboxylation and phosphorylation of OAA to form PEP were conducted in a reaction mixture containing 50 mM HEPES (pH 7.5), 10 mM DTT, 4 mM $MgCl_2$, 500 μM GTP, 1 mM ADP, 200 μM $MnCl_2$, 150 μM NADH, 30 units of LDH, 50 μg of PK, and 350 μM OAA. All enzyme-catalyzed rates that use OAA as the substrate have been corrected for the nonenzymatic decarboxylation of OAA forming pyruvate (assays A, C, and D). This assay was started by the addition of OAA to each cuvette. OAA and GTP concentrations were varied in turn to yield the respective Michaelis constants. When OAA was varied, the reaction was performed as described above. When GTP was the varied substrate, the level of $MgCl_2$ was also varied to keep a constant 4:1 ratio of metal to nucleotide. The reaction mixture was preincubated at 25 °C for 5 min prior to the addition of OAA.

Assay B ($PEP + GDP + CO_2 \rightarrow OAA + GTP$). The dephosphorylation and carboxylation of PEP to form OAA were assessed in a reaction mixture consisting of 50 mM HEPES (pH 7.5), 10 mM DTT, 4 mM $MnCl_2$, 500 μM GDP, 150 μM NADH, 2 mM PEP, 10 units of MDH, and 50 mM $KHCO_3$. This assay was started by the addition of PEPCK to the reaction mix in the cuvette. PEP, $KHCO_3$, and GDP concentrations were varied in turn to yield the respective Michaelis constants. When GDP was the varied substrate, the level of $MnCl_2$ was also varied to keep a constant metal to nucleotide ratio of 4:1. The concentration of dissolved CO_2 was calculated from the amount of added $KHCO_3$ as previously described (*28*).

Assay C ($OAA + GTP \rightarrow pyruvate + GTP + CO_2$). The decoupling of the PEPCK-catalyzed reaction (assay A) through the production of pyruvate was assessed in the same reaction mix as assay A. The only exception was that the coupling enzyme PK

and its required nucleotide (ADP) were omitted from the reaction mix so that the direct production of pyruvate by PEPCK could be monitored. Each cuvette contained 50 mM HEPES (pH 7.5), 10 mM DTT, 4 mM $MgCl_2$, 500 μM GTP, 200 μM $MnCl_2$, 150 μM NADH, 30 units of LDH, and 350 μM OAA. Each assay was initiated by the addition of OAA that was subsequently varied to yield a Michaelis constant. The reaction mixture was preincubated at 25 °C for 5 min prior to addition of OAA.

Assay D ($OAA + GDP \rightarrow pyruvate + GDP + CO_2$). The PEPCK-catalyzed decarboxylation of OAA without subsequent phosphoryl transfer was conducted under reaction conditions identical to those of assay C except that 500 μM GDP was substituted for GTP (*18*). A Michaelis constant for OAA was determined by varying the OAA concentration. Each assay was started by the addition of OAA to each cuvette. The reaction mixture was preincubated at 25 °C for 5 min prior to the addition of OAA.

Inhibitor Assays. Inhibition experiments with oxalate and PGA were conducted using assay B. A Michaelis constant for PEP was determined at several different concentrations of each inhibitor. The inhibition by βSP was carried out using assay A because βSP is a substrate for MDH. A Michaelis constant for OAA was determined at several concentration of βSP.

Data Analysis. All kinetic data were analyzed using SigmaPlot 11. In assays A−D, the slope of the line was used to calculate a rate of enzyme activity. Because of the production of pyruvate during the OAA → PEP reaction (assay A) in the A467G mutant, the data were corrected for this activity using the K_M and V_{max} values obtained for the enzyme from assay C for the A467G enzyme. These two values were used in eq 1 to calculate the theoretical rate of catalyzed pyruvate formation at each substrate concentration used in assay A for the A467G enzyme. This calculated rate was subtracted from the observed activity after correction for nonenzymatic, spontaneous OAA decarboxylation as described above. All kinetic data were fit nonlinearly to the Henri−Michaelis−Menten relationship (eq 1) to determine K_M and V_{max} values. A k_{cat} value was calculated from the V_{max} using a molecular mass of 69415 Da. For the inhibition studies, the rate of the enzyme-catalyzed reaction was calculated from the slope of the line for all data points. For the inhibition of PEPCK by PGA and oxalate, the rate data were plotted together and globally fit to eq 1, resulting in a singular value for V_{max} and $K_{M,app}$ values at each concentration of inhibitor. The resulting $K_{M,app}$ values were replotted against the concentration of inhibitor giving a linear fit to eq 2 that was used to calculate the K_i value for each inhibitor. For βSP,[2] the data at each concentration of inhibitor were fit individually to eq 1, resulting in $K_{M,app}$ and $V_{max,app}$ values. From these values, the ratio $K_{M,app}/V_{max,app}$ was calculated, and these values were plotted as a function of βSP concentration and fit to eq 3 to determine the K_i value for the competitive binding effect.

$$v = \frac{V_{max}[S]}{K_M + [S]} \quad (1)$$

[2]In our hands, βSP is observed to act as a mixed inhibitor of PEPCK against OAA that we have identified is due to contamination of our βSP preparations with low levels of chloride. Structural studies of the PEPCK−βSP complex demonstrate that this results in weak binding of chloride near the active site of PEPCK and leads to the observed mixed inhibition pattern (T. A. Johnson and T. Holyoak, unpublished data). For the purposes of this study, we report only the K_i values on the slope representing the competitive binding of βSP to the OAA site of PEPCK.

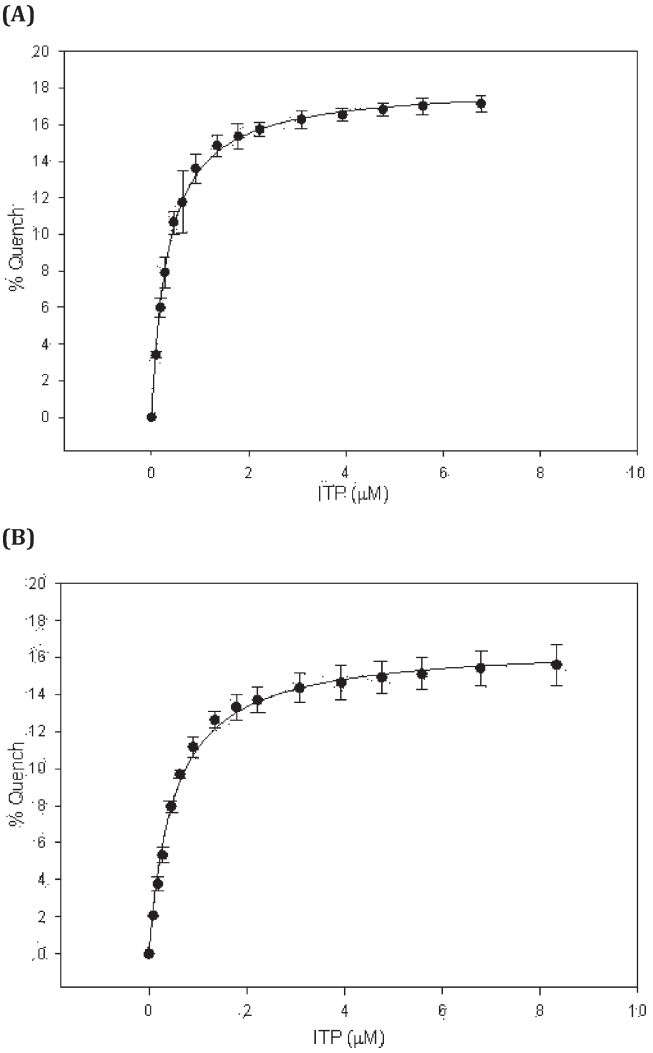

FIGURE 2: Binding isotherms illustrating the binding of ITP to (A) wild-type and (B) A467G PEPCK as measured by intrinsic protein fluorescence quenching and described in Materials and Methods.

$$K_{M,app} = \frac{K_M}{K_i}[I] + K_M \quad (2)$$

$$\frac{K_{M,app}}{V_{max,app}} = \frac{\frac{K_M}{V_{max}}}{K_i}[I] + \frac{K_M}{V_{max}} \quad (3)$$

where v is the initial velocity, V_{max} is the maximal velocity achieved, [S] is the concentration of substrate at each velocity, K_M is the Michaelis constant for each respective substrate, [I] is the inhibitor concentration, and K_i is the inhibition constant.

Fluorescence Quenching. Fluorescence quenching experiments were performed using a steady-state PTI instrument with temperature control. Each assay was conducted in a triangular cuvette at 15 °C with constant stirring. The samples contained 50 mM HEPES (pH 7.5), 10 mM DTT, 1 mM $MnCl_2$, 200 μM KCl, and PEPCK (1−5 μM). The emission was monitored at 330 nm after excitation at 295 nm. The sample was titrated with an identical solution, which also contained IDP or ITP. Inosine nucleotides were substituted for the guanosine nucleotides utilized in the kinetic studies to reduce inner filter effects. The binding constants and quenching maxima were determined by a

Table 2: Characterization of Wild-Type and A467G Cytosolic PEPCK[a]

(A) OAA + GTP → PEP + GDP + CO_2

	K_M (μM)			k_{cat}/K_M (M^{-1} s^{-1})	
enzyme	OAA	GTP	k_{cat} (s^{-1})	OAA	GTP
wild-type	52 ± 6	68 ± 4	54 ± 0.2	1.0×10^6	7.9×10^5
A467G	749 ± 67	47 ± 17	14 ± 0.1	1.9×10^4	2.7×10^5

(B) PEP + CO_2 + GDP → OAA + GTP

	K_M (μM)				k_{cat}/K_M (M^{-1} s^{-1})	
enzyme	PEP	GDP	CO_2	k_{cat} (s^{-1})	PEP	GDP	CO_2
wild-type	294 ± 16	39 ± 2	1194 ± 109	19 ± 0.8	6.6×10^4	5.1×10^5	1.6×10^4
A467G	63 ± 11	70 ± 8	814 ± 98	1 ± 0.1	1.5×10^4	1.4×10^4	1.2×10^3

(C) Pyruvate Production during the OAA + GTP → PEP + GDP + CO_2 Reaction

enzyme	K_M(OAA) (μM)	k_{cat} (s^{-1})	k_{cat}/K_M (M^{-1} s^{-1})
wild-type	ND[b]	ND[b]	ND[b]
A467G	512 ± 43	2.6 ± 0.1	5.0×10^3

(D) Decarboxylation Half-Reaction (OAA + GDP → pyruvate + GDP + CO_2)

enzyme	K_M(OAA) (μM)	k_{cat} (s^{-1})	k_{cat}/K_M (M^{-1} s^{-1})
wild-type	117 ± 11	2.3 ± 0.1	2.0×10^4
A467G	970 ± 118	1.3 ± 0.1	1.0×10^3

(E) Substrate and Substrate Analogue Affinities

enzyme	K_D(ITP) (μM)	K_D(IDP) (μM)	K_I(βSP) (μM)	K_I(PGA) (μM)	K_I(oxalate) (μM)
wild-type	0.34 ± 0.01	11.6 ± 0.4	26 ± 1	2530 ± 13	106 ± 6
A467G	0.50 ± 0.03	8.0 ± 0.3	50 ± 3	1460 ± 48	860 ± 33

[a]All experiments were performed at 25 °C. [b]No pyruvate formation detected.

nonlinear least-squares fit of the titration data to eq 4 (IDP) or eq 5 (ITP).

$$Q_L = Q_M \left\{ \left[K_D + L_T + P_T - \sqrt{(K_D + L_T + P_T)^2 - 4P_T L_T} \right] / (2P_T) \right\} \quad (4)$$

where Q_L is the quenching at each ligand concentration, Q_M is the maximal quenching observed, K_D is the dissociation constant of the complex, L_T is the ligand concentration titrated into the sample, and P_T is the protein concentration.

$$Q_L = \frac{Q_M L_T}{K_D + L_T} \quad (5)$$

where Q_L is the quenching at each ligand concentration, Q_M is the maximal quenching observed, K_D is the dissociation constant of the complex, and L_T is the ligand concentration titrated into the sample. Equation 5 was utilized for the ITP binding data as poor fits to the data were obtained using eq 4. We presume that these poor fits were the result of contamination of the ITP solution with low levels of IDP that did not allow for a discrete treatment of the distribution of species using eq 4. Representative binding isotherms for WT and A467G are shown in Figure 2.

RESULTS

Kinetic experiments were performed to determine the effect of the mutation upon the kinetic constants for the reaction in the direction of both PEP formation and OAA formation as well as the OAA decarboxylase activity (Table 2).

Kinetic Characterization of Recombinant WT and A467G PEPCK. (*i*) *OAA → PEP*. In the physiological direction, where OAA is converted to PEP, a mixed metal assay (assay A) was utilized, as the background rate of nonenzymatic OAA decarboxylation is lower in the presence of high concentrations of magnesium than in the presence of manganese as the sole divalent cation. Utilizing this assay, A467G PEPCK has a 14-fold higher K_M value for OAA than WT (Table 2A). This increase in K_M is coupled with a reduction in k_{cat} (26% of the WT value), resulting in a reduction in catalytic efficiency (k_{cat}/K_M) of nearly 2 orders of magnitude (1.9% of the WT value). Conversely, there is little change in the K_M for GTP (factor of 1.4), resulting in the $k_{cat}/K_{M,GTP}$ decreasing by a factor of < 3. As described below, A467G produces pyruvate during the turnover of OAA to PEP. The data for the formation of PEP that is coupled to pyruvate kinase and lactate dehydrogenase were corrected for this pyruvate formation activity.

(*ii*) *PEP → OAA*. In the reverse direction, PEPCK catalyzes the formation of OAA from PEP (assay B). The A467G mutant exhibited a decrease in the K_M value for PEP (21% of the WT

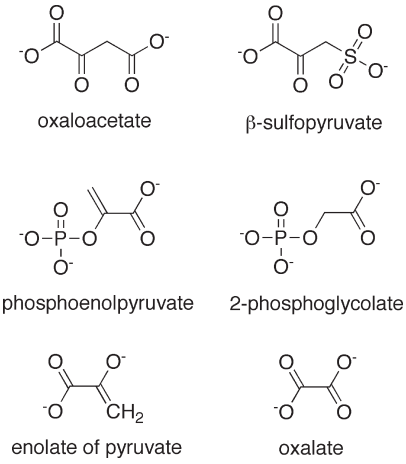

FIGURE 3: Structures of the OAA and PEP substrates and the enolate intermediate alongside the corresponding analogue utilized in these studies.

value) (Table 2B). In contrast, the A467G mutation had a k_{cat} reduced to 5% of the WT value. The combination of a decrease in K_M and a decrease in k_{cat} results in a reduction in the catalytic efficiency of A467G relative to WT by only a factor of 4. In contrast, because of a slight increase in the K_M value for GDP, k_{cat}/K_M for GDP decreases to 3% of the WT value.

(*iii*) *Pyruvate Formation*. It has been well documented that PEPCK will catalyze the production of pyruvate from OAA (*18*, *27*, *29*, *30*). With rat cPEPCK at 25 °C, this activity is dependent on the presence of GDP (assay D). Upon comparison of the mutant and WT enzymes, A467G has a K_M value 7-fold higher than that of WT, with a modest reduction in k_{cat} (57% of the WT value). This results in the WT enzyme being 20-fold more efficient at catalyzing the decarboxylation of OAA than A467G (Table 2D).

As the A467G mutation was designed to reduce the favorability of the enzyme adapting the lid-closed state and to test our proposed role for the lid in protecting the enolate intermediate, once formed, from favorable protonation (vide infra), we investigated the ability of the enzyme to catalyze the formation of pyruvate during the catalyzed formation of PEP from OAA (assay C). In the WT enzyme, there was no measurable formation of pyruvate at 25 °C. However, the A467G mutant showed a measurable amount of pyruvate formation, albeit with a K_M value similar to the elevated K_M observed in both the decarboxylation reaction and the overall reaction in the direction of PEP formation, both described above (Table 2C).

(*iv*) *Inhibition of WT and A467G PEPCK by Substrate Analogues*. The competitive inhibition of PEPCK by substrate analogues βSP and PGA and the enolate mimic oxalate has been illustrated previously on both mitochondrial and cytosolic isoforms of PEPCK (*7*, *26*). The kinetic and structural data demonstrate that all three inhibitors are excellent mimics of the respective substrate or intermediate (Figure 3). We utilized the binding constants determined from the inhibition experiments to assess whether the A467G mutation had any effect on substrate and enolate affinity. Both of the substrate analogues, βSP and PGA, have similar affinity for WT and A467G PEPCK (Table 2E). In contrast, the reduction in the affinity of oxalate with A467G (a factor of approximately 8) suggests that by extrapolation the lid mutation has decreased the stabilization of the enolate intermediate by ~5.3 kJ/mol.

(*v*) *Nucleotide Binding by Fluorescence Quenching*. The K_M values for GDP and GTP suggest that the A467G mutation has little effect on the relative affinity of PEPCK for the nucleotide substrates. This conclusion was confirmed by the direct measurement of the K_D values for IDP and ITP by intrinsic protein fluorescence quenching experiments. The inosine nucleotides were substituted in place of guanosine to reduce the inner filter effect observed when guanosine nucleotides are utilized. PEPCK utilizes inosine and guanosine nucleotides with similar catalytic efficiency, while ITC experiments with the human enzyme have demonstrated the exocyclic C-2 amino group of guanosine nucleotides increases the affinity of the enzyme for guanosine nucleotides by approximately 1 order of magnitude compared to that of the inosine analogue (*31*). As shown in Table 2E, WT PEPCK has a K_D for ITP of 0.34 μM while A467G has a K_D of 0.50 μM. Meanwhile, the dissociation constants for IDP are 11.6 and 8.0 μM for WT and A467G, respectively.

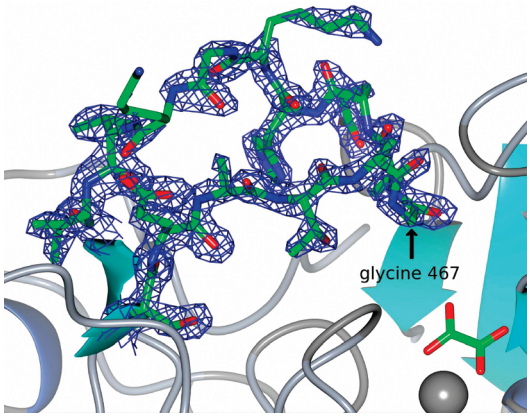

FIGURE 4: Structure of molecule A of the A467G PEPCK−oxalate−GTP complex. The partial occupancy (0.7) of the closed lid in this molecule is illustrated by the $2F_o - F_c$ density rendered at 1.3σ as a blue mesh with the corresponding lid domain rendered as a green stick model colored by atom type. The active site manganese ion and the bound oxalate molecule are rendered as a gray sphere and green stick model, respectively. The location of the A467G mutation is also labeled. Figures were generated using CCP4MG (*47*).

(*vi*) *Structures of A467G*. To demonstrate that the substitution of A467 for glycine decreases the thermodynamic favorability of the enzyme adapting the closed lid conformation but does not alter the structure that the Ω-loop adapts upon closing, we determined the structure of A467G PEPCK in complex with βSP, PGA, oxalate, and either GTP or GDP (Table 1). Identical structural studies of the WT enzyme demonstrated that as the enzyme commits to catalysis the thermodynamic favorability of the enzyme adapting the closed lid conformation increases (*9*). In the βSP−GTP and PGA−GDP structures, mimicking the Michaelis complexes for the forward and reverse reactions, respectively, the WT enzyme contains two molecules in the ASU, with one adapting a closed lid conformation and the other one remaining open. In the oxalate−GTP complex with the WT enzyme, the lid was always found to be in a closed conformation. In contrast to those results, and consistent with the design of the mutation, the structures of A467G in the βSP−GTP and PGA−GDP complexes were found to adapt only the open lid conformation, consistent with a destabilization of the closed lid state. In a similar fashion, the A467G−Mn^{2+}−oxalate−Mn^{2+}GTP structure also contains two molecules in the ASU in which molecule B possesses an open lid conformation. Molecule A was found to partially adapt a closed lid conformation that was manually adjusted to an occupancy of 70% (Figure 4). This results in an overall occupancy of the closed lid conformation for

the crystal of 35%, compared to 100% in the WT enzyme. Upon comparison of the closed lid conformation observed in molecule A with the conformation of the closed lid in the WT PEPCK−oxalate−GTP structure (PDB entry 3DT4), we observed that the substitution of glycine for alanine does not change the low-energy conformation of the closed lid (Figure 4), consistent with the observed kinetic and binding effects resulting solely from the perturbation of the thermodynamic favorability of the enzyme adapting the closed lid conformation necessary for catalysis.

DISCUSSION

The motional properties of mobile loop regions have been demonstrated in many diverse systems to be essential to enzyme function (*15*, *16*, *32*−*39*). In particular, the Ω-loop lid domain of TIM has been well characterized, and it has been demonstrated that removal of a portion of the lid leads to an increase in the production of the reaction side product methylglyoxal. Further, the removal of a portion of the lid in TIM negatively impacts catalytic function, as the lid is no longer able to stabilize the intermediate or the transition states that precede or follow its formation (*40*). In contrast, mutations in the hinge regions of the Ω-loop of TIM, designed to increase the motional freedom of the lid while negatively impacting catalytic function, do not result in an increase in the production of methylglyoxal (*32*). In general, these studies on TIM have demonstrated that the functional nature of this mobile loop domain is an exquisite balance between its rigidity and its flexibility, a property that may be a general feature of all catalytically important mobile loops (*16*, *32*, *37*). While EPR studies on *S*-adenosylmethionine synthetase (*33*) suggest that the rates of open and closed conformation sampling are identical in the presence and absence of substrates, NMR studies on TIM (*15*, *16*) as well as the crystallographic data on TIM are consistent with ligand association influencing the most stable, most highly populated conformation of the lid domain. The latter data are also consistent with the recent structural studies of PEPCK (*9*).

While PEPCK and TIM catalyze two drastically different chemical reactions, they both do so via unstable intermediate enolate species that rapidly decompose in solution. On the basis of the commonality of a lid domain, the simplest interpretation is that the mobile lid is necessary to allow ligand association or dissociation but during catalysis is required to provide an environment that sequesters and/or stabilizes the reactive intermediate and gives the enzyme the ability to follow a chemical pathway that is not available in solution due to the instability of the intermediate. Unlike the phosphate "gripper" lid domain of TIM, in PEPCK the closed lid makes no direct contacts with the bound substrates or the enolate intermediate. Therefore, in PEPCK it is not possible that new interactions between the lid and the substrates directly stabilize the lid in the closed state. In light of this observation, an alternative mechanism for describing the energetic driving force behind the transition between open and closed lid states is needed. In general, our model of lid dynamics in PEPCK proposes that not all of the free energy from substrate association is used in the formation of a tight binding E−S complex but that some of that energy is partitioned to the protein. This input energy modifies the free energy landscape that defines the conformation of the protein and results in the closed lid state becoming more thermodynamically favorable as substrates associate (*6*, *9*). This general idea has been presented previously (*41*, *42*). While the mechanism of this free energy partitioning in

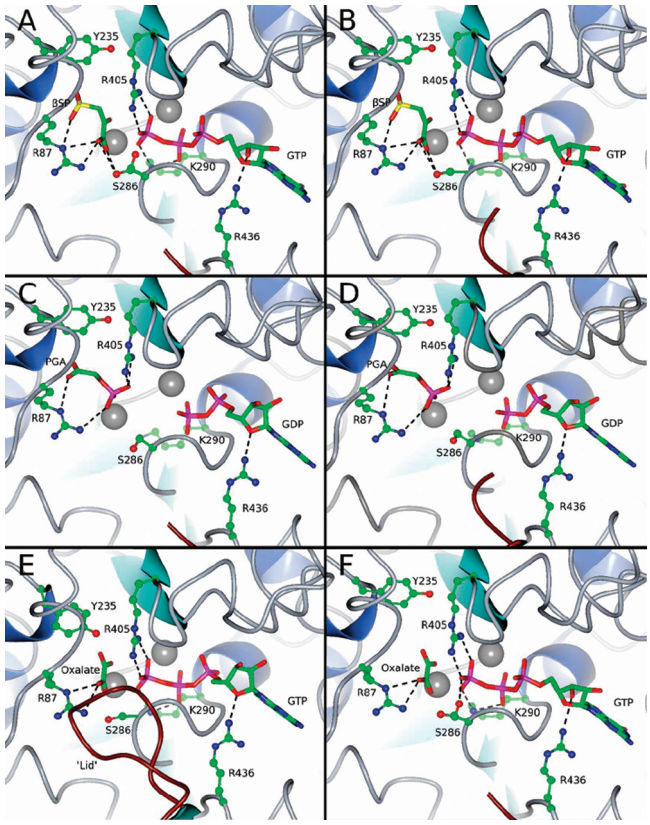

FIGURE 5: Comparison of the active sites of WT (PDB entries 3DT2, 3DT7, and 3DTB) and A467G PEPCK (PDB entries 3MOE, 3MOF, and 3MOH) in the PEPCK−Mn^{2+}−βSP−Mn^{2+}GTP [(A) WT and (B) A467G], PEPCK−Mn^{2+}−PGA−Mn^{2+}GDP [(C) WT and (D) A467G], and PEPCK−Mn^{2+}−oxalate−Mn^{2+}GTP [(E) WT and (F) A467G] complexes. All catalytic residues are rendered as ball-and-stick models colored by atom type, whereas the ligands and nucleotides (βSP, PGA, oxalate, GTP, and GDP) are rendered as thick sticks colored by atom type and labeled. Potential hydrogen bonds between the ligands and the active site residues are represented as black dashed lines. The active site and nucleotide-associated manganese ions are rendered as gray spheres, and the lid domain is colored dark red.

PEPCK is presently unknown, both the kinetic and structural data presented in this work are consistent with this model. To understand the role of the lid domain in the reaction mediated by PEPCK, we have undertaken structural and kinetic studies of a mutant of the enzyme that was designed to alter the equilibrium of the open−closed transition.

Rationale behind the A467G Mutation. To test the model of lid dynamics described above, we desired to increase the entropic penalty for lid closure while keeping the available interaction energy fixed (i.e., using the same ligands). To achieve this goal, we postulated that we could engineer a modified lid domain that, while still operating as a singular rigid domain of an Ω-loop (*13*), has an increased entropic penalty for lid ordering and closure through the introduction of a conformationally more flexible glycine residue (Figure 1). We decided that the mutation of A467 to glycine would provide such an engineered change. Upon expression and purification of this mutation (A467G), we undertook structural and functional studies to determine if the mutation provided data that were consistent with our model of loop function.

Kinetic and Structural Characterization of the A467G Mutation. (*i*) *Structures of the Michaelis and Enolate Intermediate-like Complexes*. The A467G PEPCK structures

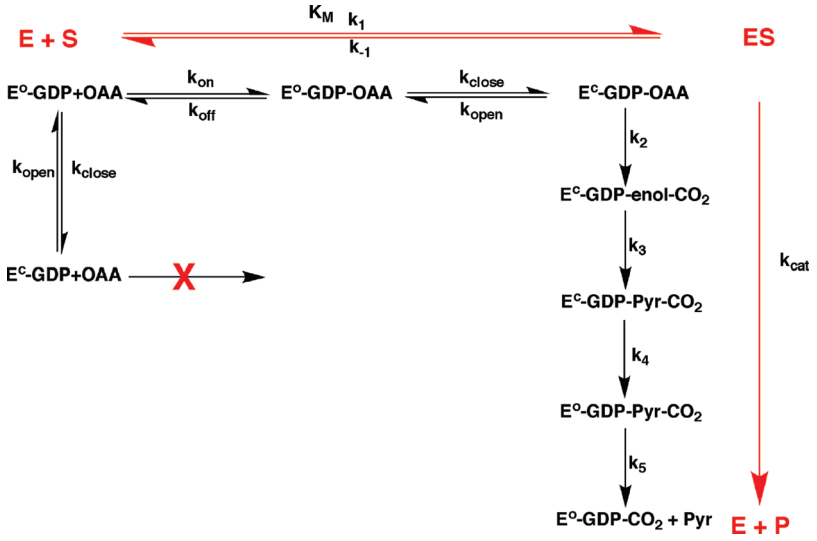

FIGURE 6: Minimal kinetic schemes for the PEPCK-catalyzed decarboxylation of OAA in the presence of GDP. In red are shown those steps corresponding to the different steady-state kinetic complexes and constants. E^o and E^c represent the lid-open and lid-closed forms of the enzyme, respectively.

mimicking the two Michaelis complexes and the enolate intermediate state, which were determined under conditions identical to those used for previous complexes with the wild-type enzyme (*9*), illustrate that no gross structural changes are induced by the lid mutation. Further, with the exception of the rotomeric state of Y235 in the A467G−oxalate−GTP complex discussed below, the enzyme−substrate contacts in the A467G complexes are identical to those in the open complexes of the WT enzyme previously determined (Figure 5). However, consistent with the design of the mutation, the introduction of the glycine linker has resulted in the lid-closed state being less thermodynamically favorable (Table 1). This results in the closed lid state only being observed at a low level in the A467G−oxalate−GTP complex, and not at all in the two Michaelis-like complexes (A467G−βSP−GTP and A467G−PGA−GDP). This contrasts identical experiments with the WT enzyme in which the Michaelis-like complexes have a 50−50 distribution of lid-open and lid-closed states and the oxalate−GTP complex possesses only a closed lid (*9*). Importantly, the population of molecules in the A467G−oxalate−GTP structure that do adapt the closed conformation demonstrates that the substitution of glycine for alanine has not changed the low-energy conformation of the lid and confirms that we can interpret our kinetic data in the context of the mutation functioning by disrupting the low-energy lid state and not having other structural effects (Figure 4). Unfortunately, the crystallographic studies do not allow us to determine whether the shift in the equilibrium for the lid conformation toward the open state is due to a decrease in the closing rate or an increase in the opening rate. Previous studies with TIM have shown that hinge mutations in the Ω-loop that result in a lid with more entropic freedom do not lead to an increased rate of lid opening but do decrease the frequency of lid closure (*16*). Therefore, further studies on PEPCK will be necessary to see what effect increasing the entropy of the lid domain has on the lid opening and closing rates.

(*ii*) *Kinetic Consequences of the Disruption of Lid Dynamics*. On the basis of the previously published structural data demonstrating that PEPCK follows an induced-fit mechanism that results in the true "E−S" complex not being formed until the lid closes (*9*), we propose the schemes illustrated in Figures 6 and 7, to interpret the kinetic data for the WT and A467G enzymes. We are well aware that these schemes are an oversimplification. A simple two-state model would result in an equilibrium defining the open and closed lid conformations of each kinetic complex, and a more realistic interpretation would be a reaction coordinate surface that defines the ensemble of protein states in the different kinetic complexes (*43*, *44*). However, we think the lowest-energy trajectory illustrated by the simple two-dimensional reaction coordinate and the schemes is reasonable for the purpose of our interpretation of the data.

(*iii*) *Lid Closure Stabilizes the Enolate Intermediate*. In the WT PEPCK−oxalate−GTP complex, Y235 is observed to occupy a rotomeric position that positions the phenolic side chain forward in the active site toward oxalate and the active site metal (*9*). In contrast, in molecule B of the A467G mutant structure, even though oxalate is bound at the active site, Y235 occupies a predominantly rearward rotomeric state. This state is observed as the predominant conformation for Y235 in other lid-open complexes of PEPCK. The coincident nature of lid closure and the stabilization of the forward rotomer of Y235 in the presence of oxalate are supported by the structure of molecule A of the A467G mutant. Molecule A possesses a mixture of lid open and closed states and also has a mixed occupancy of the forward and rearward rotomers of Y235. While the forward rotomer of Y235 cannot directly H-bond with the enolate, the altered environment created by a shift in the lid to prefer the open state in A467G PEPCK and the resulting shift in the low-energy position of Y235 appear to result in an increased K_i being observed for the A467G mutant (Table 2E). An explanation for this loss of binding energy (~5.3 kJ/mol) could be that the rearward Y235 rotomer is no longer able to provide an anion−quadrapole interaction with oxalate, an interaction that has been previously suggested to be important for interactions of PEP with PEPCK based upon an increased K_M for PEP in Y235 mutants of human cPEPCK (*29*). A related observation is that in the open A467G−oxalate−GTP complex, the rearward Y235 rotomer coincides with an altered hydration state of the bound oxalate molecule (Figure 8). This altered hydration state may contribute to the weakened affinity of the enzyme for the enolate or oxalate; however, the change in water structure could account for the formation of pyruvate in A467G such that the repositioned water

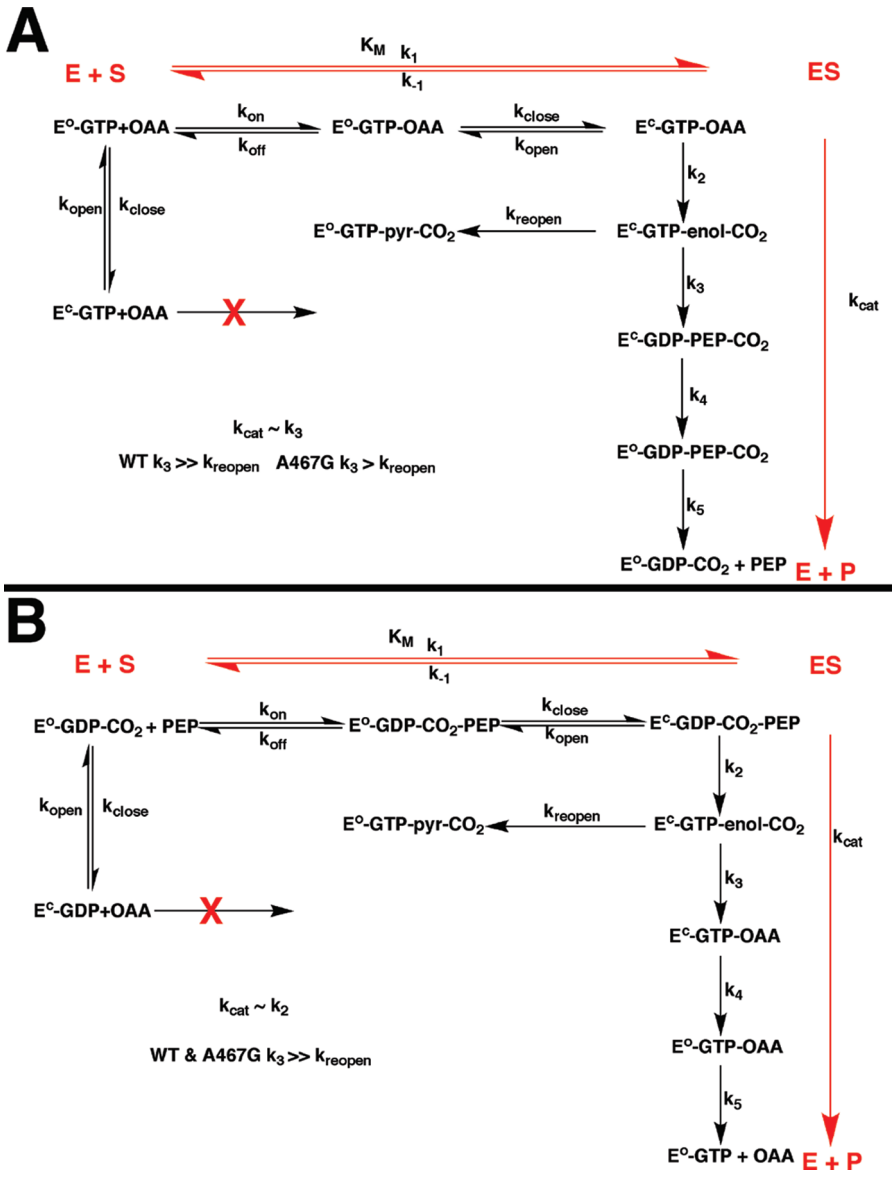

FIGURE 7: Minimal kinetic schemes for the PEPCK-catalyzed reaction in the (A) OAA → PEP direction and (B) PEP → OAA direction. In red are shown those steps corresponding to the different steady-state kinetic complexes and constants. E^o and E^c represent the lid-open and lid-closed forms of the enzyme, respectively.

molecules create an environment in which they are now able to protonate the enolate intermediate, a feature not observed in the WT enzyme at 25 °C. It is presently unknown whether the enolate is protonated on the enzyme or is released and protonated in solution. However, as pyruvate only weakly associates with PEPCK [K_i = 9 mM (*26*)], the protonation of the tightly bound enolate would provide a mechanism for its release after protonation of the enzyme. Upon examination of the kinetic data, the decrease in enolate stabilization by the shift in the equilibrium position of the lid toward an open conformation and its subsequent effect on the low-energy conformation for Y235 and the solvation of the active site have the effect of increasing the activation barrier for both phosphoryl transfer and the carboxylation–decarboxylation steps (Table 2 and Figure 9). The reduction in oxalate affinity and, by extrapolation, enolate affinity by a factor of ~8 translates into a reduction in the decarboxylation rate observed in the presence of OAA and GDP to approximately 57% of the WT rate and a reduction in the k_{cat}/K_M for this process by more than 1 order of magnitude (Table 2D). If, as discussed below, in the direction of OAA synthesis (Table 2B) k_{cat} represents the

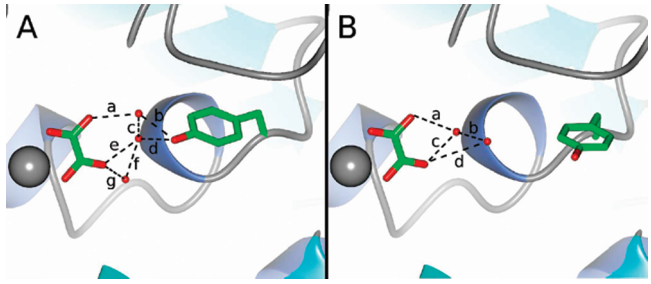

FIGURE 8: Changes in the rotomeric state of Y235 and the water structure surrounding oxalate in the (A) lid-closed WT PEPCK–Mn^{2+}–oxalate–Mn^{2+}GTP (*9*) and (B) lid-open A467G–Mn^{2+}–oxalate–Mn^{2+}GTP complexes. In panel A, the dashed lines represent potential hydrogen bonds with lengths of (a) 2.7, (b) 2.4, (c) 2.5, (d) 2.7, (e) 2.8, (f) 2.6, and (g) 3.0 Å. Similarly, in panel B, the potential hydrogen bond lengths are (a) 3.3,Å (b) 2.5, (c) 2.7, and (d) 3.4 Å. On the basis of structural work by Cotelesage et al. (*48*), we propose that the water molecules separated by distance c in panel A define the CO_2 binding site. As illustrated in panel B, this binding site for CO_2 is only present in the lid-closed conformation shown in panel A.

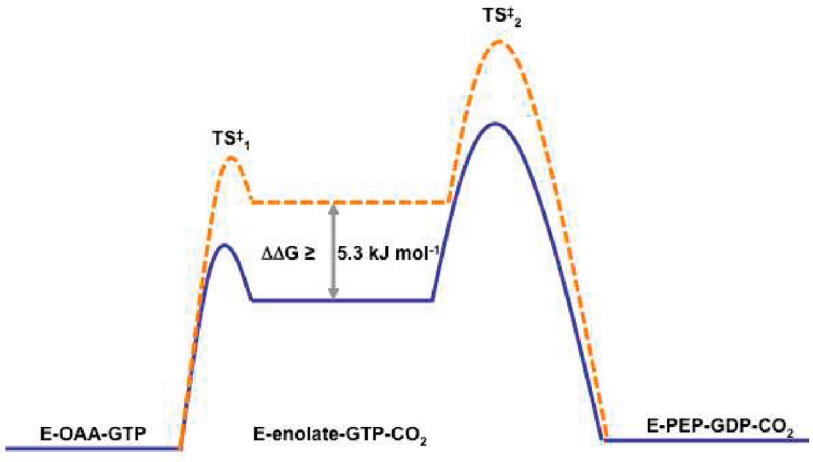

FIGURE 9: Cartoon reaction coordinate for WT (blue solid line) and A467G (orange dashed line) PEPCK based upon the differential inhibition of the two enzyme forms by the enolate intermediate analogue, oxalate.

phosphorylation of GDP by PEP to form the enolate intermediate, this reduction in oxalate affinity would translate into a reduction in the phosphoryl transfer rate to 5% of that for the WT enzyme (Table 2B). Interpreted in this way, the structural data for the A467G−Mn^{2+}−oxalate−Mn^{2+}GTP complex agree with the kinetic data. If the intermediate destabilization (~5.3 kJ/mol) is fully expressed in either transition state, this would result in a reduction in the rate of catalysis by a factor of 10, a value similar in magnitude to the results of the steady-state data presented above (Table 2). It should be noted that absolute discrepancies between the oxalate affinity data and the kinetic data could be the result of not knowing the extent to which oxalate mimics the actual enolate intermediate [similar to studies of TIM (*40*)], and therefore, the change in oxalate affinity is only a qualitative measure of the potential change in enolate affinity. Further, we do not know whether the same destabilization of the enolate intermediate would be fully expressed in either or both of the two transition states. Finally, the exact nature of the rate-limiting step(s) in WT and A467G is unknown. Our interpretation does provide a reasonable explanation of how the destabilization of the closed lid conformation leads to both a defect in catalysis and the propensity to generate pyruvate.

The interpretation of the kinetic data given above also relies on k_{cat} not being limited by the lid open/close rate in PEPCK. This would be in contrast to TIM. TIM, however, operates at a much higher catalytic efficiency, and the open−closed transition of the phosphate gripper loop occurs on that same time scale (~10^4 s^{-1}) (*15*, *45*). This rate is approximately 3 orders of magnitude faster than the k_{cat} in PEPCK, supporting our assumption that k_{cat} does not represent the open−closed transition in PEPCK. Further, as the effect of A467G on k_{cat} is larger in the direction of OAA synthesis than in the direction of PEP synthesis, the asymmetry provides additional support for the possibility that the phosphoryl transfer reaction is at least partially rate limiting, consistent with the reaction coordinate diagram in Figure 9.

(*iv*) *Decarboxylation of OAA*. In addition to the modest change in the decarboxylation rate observed in the decarboxylation half-reaction, there is a modest increase (~8-fold) in the K_M for OAA in this reaction (Table 2D). As illustrated in Figure 6, this K_M value represents both binding of OAA to the PEPCK−GDP complex and the opening and closing of the lid. This conclusion is reached on the basis of two pieces of data. (1) Previous structural studies of the PEPCK−OAA−GDP complex demonstrate that this ligation state of the enzyme has an increased propensity to form the closed lid conformation, similar to the PEPCK−βSP−GTP and PEPCK−PGA−GDP Michaelis complex mimics (*8*). (2) With the rat cPEPCK, at 25 °C, the decarboxylation activity is observed only in the presence of diphosphate nucleotide.

Both of these pieces of data are consistent with the idea that lid closure is required to initiate the decarboxylation reaction. Our model for the decarboxylation activity is one, similar to formation of the Michaelis complexes, in which formation of the PEPCK−OAA−GDP complex results in a shift in the open−closed equilibrium to the right and this leads to the generation of the enolate and CO_2. However, as there is no phosphoryl donor present to phosphorylate the intermediate, pyruvate is formed and released the next time the lid samples the open conformation. Therefore, on the basis of the scheme illustrated in Figure 6, the observed increase in the K_M value could result from either an increase in k_2, k_{open}, or k_{off} or a decrease in k_{on} or k_{close}. As the observed reduction in k_2 from the decarboxylation data is in the wrong direction to cause an increase in K_M, an alternate explanation is needed. The inhibition of PEPCK by βSP suggests that k_{on} and k_{off} are only modestly affected, since the binding of βSP in WT and A467G differs by a factor of only ~2. This modest effect on binding could be the result of altering lid dynamics in the PEPCK−GTP or −GDP state (Figure 6) such that the altered opening and/or closing rates affect k_{on}/k_{off} as the structural studies demonstrate that binding of substrates to PEPCK cannot occur after lid closure (*9*). This type of perturbed lid behavior, prior to formation of the Michaelis complex, has also been used to explain the kinetic data of hinge mutations of TIM (*16*). Therefore, the structural and kinetic data are consistent with the observed increase in K_M resulting from either a reduction in the rate of the transition to the closed conformation or an increase in the frequency of lid opening, which results in the open−closed equilibrium shifting to the left, resulting in an elevated K_M value for OAA.

(*v*) *OAA → PEP Reaction*. Similar to what is discussed above for the decarboxylation half-reaction, a modest reduction in k_{cat} (26% of the WT rate) and an increase (14-fold) in the K_M for OAA are observed. On the basis of the interpretation provided above, we again conclude that the change in the K_M value is due to either a decrease in the rate of lid closure or an

increase in the rate of lid opening, resulting in the equilibrium for the closed lid conformation shifting to the left which is consistent with both the design of the mutation and the structural data. Again, assuming that $k_{cat} \sim k_3$ [the phosphorylation of the enolate by GTP (Figure 7A)], we conclude that this shift in the favorability of lid closing has a modest effect on the activation energy for the reaction as illustrated in Figure 9 and described above. The observation of the formation of pyruvate by the enzyme during turnover to PEP suggests that, while in the wild-type enzyme k_3 is fast relative to k_{reopen} (no formation of pyruvate observed), either the reduction in the phosphoryl transfer rate, through the destabilization of the enolate, or an increase in the rate of lid opening results in the rate of phosphoryl transfer becoming closer to the rate of opening, such that now for every five PEP molecules produced one pyruvate molecule is formed (Table 2 and Figure 7A). To address the possibility that a slowing of the phosphoryl transfer rate results in the observed production of pyruvate, we conducted kinetic studies with WT PEPCK using the slow substrate guanosine 5′-*O*-(γ-thio)triphosphate (GTPγS). Consistent with previous studies using ITPγS (*46*), the use of GTPγS reduces k_{cat} (13 s^{-1}) and the K_M for GTPγS is 39 μM. Using GTPγS, we did not observe any pyrvuate formation during the OAA → PEP reaction. Therefore, the data suggest that making phosphoryl transfer solely or more rate-limiting does not result in any decoupling of the reaction to pyruvate and that simply slowing the phosphoryl transfer rate in the absence of a destabilization of the lid-closed conformation is not sufficient to decouple the reaction.

(*vi*) *PEP → OAA Reaction*. In contrast to the decarboxylation reaction and the reaction in the direction of PEP formation, the reaction in the direction of OAA formation results in a reduction in the K_M for PEP (~21% of the K_M for WT) and a more drastic reduction in k_{cat} (~5% of that for WT). Again, we can interpret the data in the context of the model presented in Figure 7B. On the basis of the inhibition data using the PEP analogue PGA, we see that the decrease in the K_M value with A467G is not due to solely to an increase in the affinity of the enzyme for PEP as the affinity of the enzyme for PGA increases by a factor of < 2 (Table 2E). In the direction of OAA synthesis, rather than lid closure initiating decarboxylation and the formation of the enolate, in this direction (PEP → OAA) lid closure stimulates the transfer of a phosphoryl group from PEP to GDP, forming the enolate intermediate since lid closure is necessary for PEP to adopt a kinetically competent conformation for phosphoryl transfer (*9*). On the basis of the standard free energies for the reaction, we envision this to be a more energetically costly reaction (Figure 9) (*6*). As a consequence, the destabilization of the enolate has a more drastic effect on the activation energy barrier for the reaction in this direction and results in k_{cat} being reduced to 5% of the WT value. This reduction in k_{cat} (k_2) leads to the observed reduction in K_M, as the observed K_M value for A467G shifts in a direction toward the true K_D for PEP. As the other kinetic and structural data presented here suggest that lid opening and closing are perturbed by the A467G mutation, the true K_D for PEP should be lower than the K_M of 60 μM observed as the change in the position of the open−closed equilibrium for the lid may still result in conditions that are not at rapid equilibrium. This interpretation is also consistent with the lack of observed pyruvate production during turnover in this reaction direction. Again on the basis of our free energy diagram (Figure 9), our model and data suggest that in the PEP → OAA direction the slow step, phosphoryl transfer, precedes enolate formation, and therefore, if as expected carboxylation (k_3) is significantly faster than the reopening rate, this would result in the absence of pyruvate production in this direction (Figure 7B). Alternatively, the high concentrations of CO_2 present in the reaction assay in this direction could result in an A467G−Mn^{2+}−enolate−CO_2−Mn^{2+}GTP complex that alters the solvation of the enolate intermediate in much the same way as the altered rotomeric state of Y235 that coincides with the lid open enzyme does. On the basis of this interpretation, even though the lid-closed conformation of PEPCK is destabilized by the A467G mutation, the water structure in the A467G−enolate−CO_2−GTP complex is not conducive to enolate protonation. This model would require that the enolate complex arising from the decarboxylation of OAA rapidly lose CO_2 during the transition to the closed A467G−Mn^{2+}−enolate−Mn^{2+}GTP complex. This would be consistent with the weak affinity of the enzyme for CO_2. In this direction, the resulting A467G−Mn^{2+}−enolate−Mn^{2+}GTP complex would possess a water structure similar to the A467G−Mn^{2+}−oxalate−Mn^{2+}GTP structure that we propose allows for protonation of the enolate (Figure 8B). Arguing against this latter model is the observation that when using assay conditions with subsaturating concentrations of CO_2 we are still unable to detect pyruvate formation in the PEP → OAA direction (data not shown). On the basis of all of the information, we suggest it is most likely that the competing rates between phosphoryl transfer and lid reopening result in the decoupling of the PEPCK reaction with the A467G mutation; however, more work is obviously necessary to clarify the mechanism by which A467G produces pyruvate during the OAA → PEP conversion and the lack of this activity in the opposite direction.

CONCLUSION

Perhaps not surprisingly, the lid domain of PEPCK has a general function similar to that of the lid domain found in TIM. It operates both to sequester the reactive intermediate from alternate chemistries and to stabilize the enolate intermediate. In contrast to TIM, this stabilization of the enolate by the closed lid facilitates the chemical conversion of substrates to products without the enzyme directly interacting with the substrates. The structural and kinetic characterization of A467G is consistent with the mutation causing a perturbation in the equilibrium position of the lid toward the open state, consistent with the mutation increasing the conformational entropy of the domain and resulting in the decoupling of the reaction through the formation of pyruvate. In addition, this shift in the conformational equilibrium of the lid domain results in the loss of the Y235−enolate interaction which hampers the ability of the enzyme to stabilize the bound enolate and subsequently the transition states that precede and follow its formation and results in catalytic defect.

ACKNOWLEDGMENT

We thank Dr. Aron Fenton and Ms. Sarah Sullivan for their helpful suggestions during the preparation of the manuscript.

REFERENCES

1. Lee, M. H., Hebda, C. A., and Nowak, T. (1981) The Role of Cations in Avian Liver Phosphoenolpyruvate Carboxykinase Catalysis. Activation and Regulation. *J. Biol. Chem. 256*, 12793–12801.
2. Colombo, G., Carlson, G. M., and Lardy, H. A. (1981) Phosphoenolpyruvate Carboxykinase (Guanosine 5′-Triphosphate) from Rat Liver Cytosol. Dual-Cation Requirement for the Carboxylation Reaction. *Biochemistry 20*, 2749–2757.

3. Hebda, C. A., and Nowak, T. (1982) The Purification, Characterization, and Activation of Phosphoenolpyruvate Carboxykinase from Chicken Liver Mitochondria. *J. Biol. Chem. 257*, 5503–5514.
4. Hebda, C. A., and Nowak, T. (1982) Phosphoenolpyruvate Carboxykinase. Mn^{2+} and Mn^{2+} Substrate Complexes. *J. Biol. Chem. 257*, 5515–5522.
5. Yang, J., Kalhan, S. C., and Hanson, R. W. (2009) What Is the Metabolic Role of Phosphoenolpyruvate Carboxykinase? *J. Biol. Chem. 284*, 27025–27029.
6. Carlson, G. M., and Holyoak, T. (2009) Structural Insights into the Mechanism of Phosphoenolpyruvate Carboxykinase Catalysis. *J. Biol. Chem. 284*, 27037–27041.
7. Stiffin, R.-M., Sullivan, S. M., Carlson, G. M., and Holyoak, T. (2008) Differential Inhibition of Cytosolic Pepck by Substrate Analogues. Kinetic and Structural Characterization of Inhibitor Recognition. *Biochemistry 47*, 2099–2109.
8. Sullivan, S. M., and Holyoak, T. (2007) Structures of Rat Cytosolic Pepck: Insight into the Mechanism of Phosphorylation and Decarboxylation of Oxaloacetic Acid. *Biochemistry 46*, 10078–10088.
9. Sullivan, S. M., and Holyoak, T. (2008) Enzymes with Lid-Gated Active Sites Must Operate by an Induced Fit Mechanism Instead of Conformational Selection. *Proc. Natl. Acad. Sci. U.S.A. 105*, 13829–13834.
10. Alber, T., Banner, D. W., Bloomer, A. C., Petsko, G. A., Phillips, D., Rivers, P. S., and Wilson, I. A. (1981) On the Three-Dimensional Structure and Catalytic Mechanism of Triose Phosphate Isomerase. *Philos. Trans. R. Soc. London, Ser. B 293*, 159–171.
11. Banner, D. W., Bloomer, A. C., Petsko, G. A., Phillips, D. C., Pogson, C. I., Wilson, I. A., Corran, P. H., Furth, A. J., Milman, J. D., Offord, R. E., Priddle, J. D., and Waley, S. G. (1975) Structure of Chicken Muscle Triose Phosphate Isomerase Determined Crystallographically at 2.5 Angstrom Resolution Using Amino Acid Sequence Data. *Nature 255*, 609–614.
12. Lolis, E., and Petsko, G. A. (1990) Crystallographic Analysis of the Complex between Triosephosphate Isomerase and 2-Phosphoglycolate at 2.5-Å Resolution: Implications for Catalysis. *Biochemistry 29*, 6619–6625.
13. Joseph, D., Petsko, G. A., and Karplus, M. (1990) Anatomy of a Conformational Change: Hinged "Lid" Motion of the Triosephosphate Isomerase Loop. *Science 249*, 1425–1428.
14. Fersht, A. R. (1974) Catalysis, Binding and Enzyme-Substrate Complementarity. *Proc. R. Soc. London, Ser. B 187*, 397–407.
15. Williams, J. C., and McDermott, A. E. (1995) Dynamics of the Flexible Loop of Triosephosphate Isomerase: The Loop Motion Is Not Ligand Gated. *Biochemistry 34*, 8309–8319.
16. Kempf, J. G., Jung, J. Y., Ragain, C., Sampson, N. S., and Loria, J. P. (2007) Dynamic Requirements for a Functional Protein Hinge. *J. Mol. Biol. 368*, 131–149.
17. Griffith, O. W., and Weinstein, C. L. (1987) β-Sulfopyruvate. *Methods Enzymol. 143*, 221–223.
18. Colombo, G., Carlson, G. M., and Lardy, H. A. (1978) Phosphoenolpyruvate Carboxykinase (Guanosine Triphosphate) from Rat Liver Cytosol. Separation of Homogeneous Forms of the Enzyme with High and Low Activity by Chromatography on Agarose-Hexane-Guanosine Triphosphate. *Biochemistry 17*, 5321–5329.
19. Otwinowski, Z., and Minor, W. (1997) Processing of X-Ray Diffraction Data Collected in Oscillation Mode. *Methods Enzymol. 276*, 307–326.
20. Vagin, A., and Teplyakov, A. (1997) Molrep: An Automated Program for Molecular Replacement. *J. Appl. Crystallogr. 30*, 1022–1025.
21. Bailey, S. (1994) The Ccp4 Suite: Programs for Protein Crystallography. *Acta Crystallogr. D50*, 760–763.
22. Emsley, P., and Cowtan, K. (2004) Coot: Model-Building Tools for Molecular Graphics. *Acta Crystallogr. D60*, 2126–2132.
23. Painter, J., and Merritt, E. A. (2005) A Molecular Viewer for the Analysis of Tls Rigid-Body Motion in Macromolecules. *Acta Crystallogr. D61*, 465–471.
24. Painter, J., and Merritt, E. A. (2006) Optimal Description of a Protein Structure in Terms of Multiple Groups Undergoing Tls Motion. *Acta Crystallogr. D62*, 439–450.
25. Painter, J., and Merritt, E. A. (2006) Tlsmd Web Server for the Generation of Multi-Group Tls Models. *J. Appl. Crystallogr. 39*, 109–111.
26. Ash, D. E., Emig, F. A., Chowdhury, S. A., Satoh, Y., and Schramm, V. L. (1990) Mammalian and Avian Liver Phosphoenolpyruvate Carboxykinase: Alternate Substrates and Inhibition by Analogs of Oxaloacetate. *J. Biol. Chem. 265*, 7377–7384.
27. Noce, P. S., and Utter, M. F. (1975) Decarboxylation of Oxalacetate to Pyruvate by Purified Avian Liver Phosphoenolpyruvate Carboxykinase. *J. Biol. Chem. 250*, 9099–9105.
28. Holyoak, T., and Nowak, T. (2004) pH Dependence of the Reaction Catalyzed by Avian Mitochondrial Phosphoenolpyruvate Carboxykinase. *Biochemistry 43*, 7054–7065.
29. Dharmarajan, L., Case, C. L., Dunten, P., and Mukhopadhyay, B. (2008) Tyr235 of Human Cytosolic Phosphoenolpyruvate Carboxykinase Influences Catalysis through an Anion-Quadrupole Interaction with Phosphoenolpyruvate Carboxylate. *FEBS J. 275*, 5810–5819.
30. Jabalquinto, A. M., Laivenieks, M., Zeikus, J. G., and Cardemil, E. (1999) Characterization of the Oxaloacetate Decarboxylase and Pyruvate Kinase-Like Activities of *Saccharomyces cerevisiae* and *Anaerobiospirillum succiniciproducens* Phosphoenolpyruvate Carboxykinases. *J. Protein Chem. 18*, 659–664.
31. Dunten, P., Belunis, C., Crowther, R., Hollfelder, K., Kammlott, U., Levin, W., Michel, H., Ramsey, G. B., Swain, A., Weber, D., and Wertheimer, S. J. (2002) Crystal Structure of Human Cytosolic Phosphoenolpyruvate Carboxykinase Reveals a New Gtp-Binding Site. *J. Mol. Biol. 316*, 257–264.
32. Xiang, J., Jung, J. Y., and Sampson, N. S. (2004) Entropy Effects on Protein Hinges: The Reaction Catalyzed by Triosephosphate Isomerase. *Biochemistry 43*, 11436–11445.
33. Taylor, J. C., and Markham, G. D. (2003) Conformational Dynamics of the Active Site Loop of S-Adenosylmethionine Synthetase Illuminated by Site-Directed Spin Labeling. *Arch. Biochem. Biophys. 415*, 164–171.
34. Hedstrom, L., Szilagyi, L., and Rutter, W. J. (1992) Converting Trypsin to Chymotrypsin: The Role of Surface Loops. *Science 255*, 1249–1253.
35. Johnson, T. A., Qiu, J., Plaut, A. G., and Holyoak, T. (2009) Active-Site Gating Regulates Substrate Selectivity in a Chymotrypsin-Like Serine Protease the Structure of *Haemophilus influenzae* Immunoglobulin A1 Protease. *J. Mol. Biol. 389*, 559–574.
36. Perona, J. J., and Craik, C. S. (1997) Evolutionary Divergence of Substrate Specificity within the Chymotrypsin-Like Serine Protease Fold. *J. Biol. Chem. 272*, 29987–29990.
37. Watt, E. D., Shimada, H., Kovrigin, E. L., and Loria, J. P. (2007) The Mechanism of Rate-Limiting Motions in Enzyme Function. *Proc. Natl. Acad. Sci. U.S.A. 104*, 11981–11986.
38. Sampson, N. S., and Knowles, J. R. (1992) Segmental Motion in Catalysis: Investigation of a Hydrogen Bond Critical for Loop Closure in the Reaction of Triosephosphate Isomerase. *Biochemistry 31*, 8488–8494.
39. Sampson, N. S., and Knowles, J. R. (1992) Segmental Movement: Definition of the Structural Requirements for Loop Closure in Catalysis by Triosephosphate Isomerase. *Biochemistry 31*, 8482–8487.
40. Pompliano, D. L., Peyman, A., and Knowles, J. R. (1990) Stabilization of a Reaction Intermediate as a Catalytic Device: Definition of the Functional Role of the Flexible Loop in Triosephosphate Isomerase. *Biochemistry 29*, 3186–3194.
41. Fisher, H. F. (1988) A Unifying Model of the Thermodynamics of Formation of Dehydrogenase-Ligand Complexes. *Adv. Enzymol. Relat. Areas Mol. Biol. 61*, 1–46.
42. Jencks, W. P. (1975) Binding Energy, Specificity, and Enzymic Catalysis: The Circe Effect. *Adv. Enzymol. Relat. Areas Mol. Biol. 43*, 219–410.
43. Swint-Kruse, L., and Fisher, H. F. (2008) Enzymatic Reaction Sequences as Coupled Multiple Traces on a Multidimensional Landscape. *Trends Biochem. Sci. 33*, 104–112.
44. Benkovic, S. J., Hammes, G. G., and Hammes-Schiffer, S. (2008) Free-Energy Landscape of Enzyme Catalysis. *Biochemistry 47*, 3317–3321.
45. Rozovsky, S., Jogl, G., Tong, L., and McDermott, A. E. (2001) Solution-State NMR Investigations of Triosephosphate Isomerase Active Site Loop Motion: Ligand Release in Relation to Active Site Loop Dynamics. *J. Mol. Biol. 310*, 271–280.
46. Konopka, J. M., Lardy, H. A., and Frey, P. A. (1986) Stereochemical Course of Thiophosphoryl Transfer Catalyzed by Cytosolic Phosphoenolpyruvate Carboxykinase. *Biochemistry 25*, 5571–5575.
47. Potterton, L., McNicholas, S., Krissinel, E., Gruber, J., Cowtan, K., Emsley, P., Murshudov, G. N., Cohen, S., Perrakis, A., and Noble, M. (2004) Developments in the Ccp4Molecular-Graphics Project. *Acta Crystallogr. D60*, 2288–2294.
48. Cotelesage, J. J. H., Puttick, J., Goldie, H., Rajabi, B., Novakovski, B., and Delbaere, L. T. J. (2007) How Does an Enzyme Recognize CO_2? *Int. J. Biochem. Cell Biol. 39*, 1204–1210.